In situ synthesis of gold nanoparticles in polymer films under concentrated sunlight: control of nanoparticle size and shape with solar flux

E. Nadal, Noémi Barros, Laurent Peres, V. Goetz, Marc Respaud, Aikaterini Soulantika, H. Kachachi

In situ synthesis of gold nanoparticles in polymer films under concentrated sunlight: control of nanoparticle size and shape with solar flux

E. Nadal[a,b]†, N. Barros[a,b], L. Peres[c], V. Goetz[b], M. Respaud[d], K. Soulantica[d] and H. Kachachi[a,b]

[a]*University of Perpignan Via Domitia (UPVD), 52 Avenue Paul Alduy, 66100 Perpignan, France.*
[b]*PROMES, CNRS (UPR8521), Rambla de la thermodynamique, 66100, Perpignan, France.*
[c]*Laboratoire de Chimie de Coordination, CNRS, LCC, 205, Route de Narbonne, F-31077 Toulouse, France.*
[d]*LPCNO, Université de Toulouse, CNRS, INSA, UPS, 135 avenue de Rangueil, 31077 Toulouse, France.*

† Corresponding author: elie.nadal@univ-perp.fr

Abstract: We propose an original technique for synthesizing plasmonic nanocomposites under concentrated sunlight. Polymer films doped with gold salts are prepared by spin-coating; the nanoparticle growth is triggered within the polymer matrix by exposing the film to concentrated solar irradiation. For the first time, we demonstrate that the variation of solar flux alone allows for controlling the nanoparticles size distribution and shape and, thereby, the final plasmonic response of the composite. Interestingly, thanks to this optical approach, the *in operando* measure of the spectroscopic response permits to follow the growth of the nanoparticles in real time. The experimental results give us entails about the differences in the nanoparticle growth mechanisms at different solar fluxes. At high flux, small nanospheres with diameter centered around 3 nm to 6 nm are formed. At lower flux, bigger nanoprisms of 12 nm -18 nm are synthesized. The mechanisms are discussed and different pathways are envisaged. Finally, we demonstrate the possibility to perform a fully green synthesis by using our method to grow gold nanoparticles in a bio-polymer.

Introduction

Nanocomposites are valuable materials with new and controlled physical properties. Among them, plasmonic nanocomposites are of special interest in many applications[1]. Indeed, due to their strong absorption in the visible range combined with large field enhancement in the nanoparticle vicinity, plasmonic systems can be used in several areas such as, biology[2], sensing[3–6], optical data storage[7], in the design of metamaterials[8,9], photocatalysis[10–13] and in photovoltaic systems[14,15]. Regarding the latter, some studies have demonstrated the possibility to increase the efficiency of organic or perovskite solar cells by incorporating plasmonic nanoparticles in the active layer[16–19] or more recently to use plasmonic nanocomposites in order to design new types of luminescent solar concentrators[20,21].

Consequently, there is a real need for simple and efficient fabrication methods for this type of materials. Indeed, even if numerous fabrication approaches already exist, only a few do comply with the constraints of the solar industry that require synthesizing composites with controlled properties, over large surfaces and at low cost[22].
Regarding nanocomposite thin films based on metallic fillers in polymer matrices, most of the synthesis approaches are based on the insertion of pre-synthesized nanostructures, for which numerous method exist[23,24], into polymer solutions[25,26]. In this case, it is challenging to prevent the formation of nanoparticle aggregates and, for this reason, the use of stabilizing agents is required to obtain homogeneously dispersed nanoparticles[27]. Moreover, it is difficult to maintain a homogeneous spatial distribution at large scales using standard procedures such as coating or evaporation. These drawbacks may directly affect the optical properties of the system[28], notably by inducing a large broadening of the plasmon resonance peak.

To address these challenges of cost, complexity and up-scaling, the *in situ* synthesis approach seems appropriate. Indeed, this technique consists in growing the nanoparticles directly inside a solid polymeric matrix, previously doped with a molecular metal precursor. This allows for separating the polymer-shaping process from the control of nanoparticle dispersion inside the matrix. In this type of approach, the metal salt reduction and the nanoparticle formation can be triggered by several means such as chemical treatment[29–31], annealing of the films[31–34] or UV irradiation[35–37]. So far, this approach has proven its efficiency for producing homogeneous gold[32,35]and silver[29,38,39] nanocomposite films with high filling fractions, but a systematic control of the nanoparticle size and shape is still challenging. Porel *et al* have studied the annealing route and have shown that varying simultaneously the metal/polymer ratio and the annealing temperature permits to selectively synthesize different types of polygonal nanoplates[32]. However, this approach is limited to low metal filling fractions and does not allow for a control of the nanoparticles size. Regarding the irradiation route, Balan *et al* have shown that adding photosensitive chemical agents to the metal/polymer mixture and activating them upon UV irradiation can also allow a certain degree of control of the nanoparticle shape[40]. This elegant strategy, however, strongly increases the complexity of the system. Indeed, it is difficult to find precursors, polymers and photosensitizers that are compatible and miscible. In fact, this impairs the versatility and the simplicity of this method. Consequently, there is still a need to develop low-cost, *in situ* synthesis approaches, compatible with *(i)* the synthesis of homogeneous nanocomposite films over large areas and *(ii)* the systematic control of the nanoparticles morphologies, and consequently, their optical properties. In particular, today, there is no method that allows for a control of the morphology without modifying the intrinsic parameters of the films, i.e. by adding chemical agents to the mixture or modifying the metal/polymer ratio.

In a previous study, we demonstrated that it is possible to generate the photo-reduction of gold precursors using low-intensity, continuous visible laser irradiation at 473 nm, even if the precursor is transparent at this wavelength[41]. A subsequent annealing step induces the nanoparticle growth. In this study, we use concentrated solar irradiation (CSI) for driving the *in situ* synthesis of nanoparticles in polymers under visible light irradiation. It turns out that concentrated sunlight offers the advantage of performing both photo-reduction and annealing simultaneously, thus allowing for a 'one-step' *in situ* synthesis of nanoparticles. CSI has already proved successful in the past as a tool to promote the synthesis of high-quality nanostructures. For instance, Flamant *et al.* have pioneered this field demonstrating the

possibility to fabricate carbon nanotubes or fullerenes[42,43] by triggering thermal decomposition of graphite at very high temperature (upon irradiating with concentration factors up to 15 000 suns) and under controlled atmosphere. More recently, Gordon et *al*., have revived this approach for synthesizing original nanostructures of MoS_2 and WS_2[44–46].
In this study, we use CSI in milder conditions, working at much lower irradiation concentration under ambient-air, without inducing thermal decomposition This offers the possibility to treat a great variety of materials and potentially on very large areas. We demonstrate how CSI can be combined with the *in situ* synthesis technique to produce controlled gold nanocomposites. In particular, we demonstrate the possibility to control the nanoparticle size distribution by adjusting the intensity of the CSI (i.e concentration factor). Moreover, to better understand the formation process of the nanoparticles, we use *in operando* spectroscopic measurements allowing to monitor the growth of the nanoparticles in real time. Possible mechanisms accounting for the differences observed in the nanocomposites depending on irradiation conditions are discussed. Finally, we show that it is possible to perform a fully green synthesis by applying our method to a biopolymer and water as a solvent.

Material and methods

Doped polymer films are prepared by solubilizing chloroauric acid and a polymer (PMMA or Potato Starch) in an appropriate solvent (respectively Ethyl lactate or water) so as to obtain a 20 w% metal loading in the final composite. The mixture is then deposited by spin coating on glass wafers. The thickness of the films is about 500 nm. A detailed description of the film preparation procedure, thickness measurement along with the chemicals used can be found in Section A.1 of SI. The nanoparticles are then formed in the polymer matrix from the metallic ions when exposed to CSI. The main steps of the fabrication procedure are sketched in Fig.1.

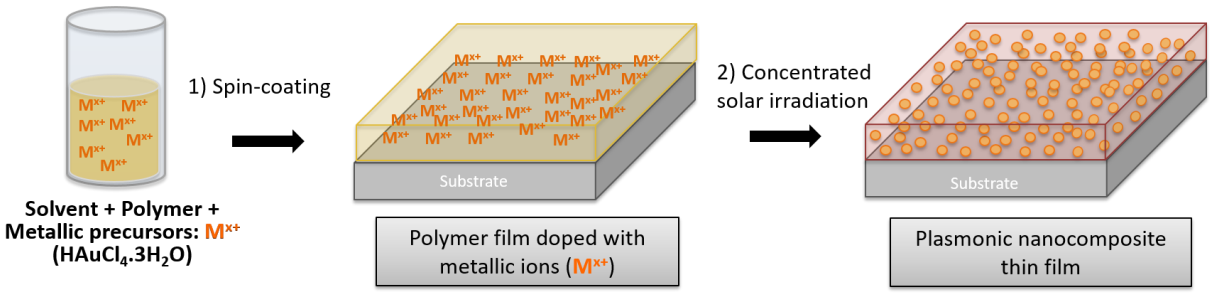

Figure 1: Main steps of the fabrication of plasmonic nanocomposites under concentrated solar irradiation

Our experimental setup for irradiation, shown in Fig.2, can be summarized as follows. A solar simulator (Oriel 91193 equipped with a 1.5 AM Global filter) producing a collimated light beam with a diameter of 30 cm simulates the sunlight. A Fresnel lens focuses the beam onto a homogenization rod. The latter homogenizes the irradiation beam, and the light flux at its output reaches concentration factors up to 50 suns. This was the maximal flux attainable in our setup. The Fresnel lens and the homogenization rod cut off the UV part of sunlight, so that the final beam is almost only composed of visible light (See section A.2 in SI).

The sample is fixed on a metallic holder whose temperature is monitored with a K-type thermocouple during the irradiation process. Due to the numerical aperture of the homogenization rod, the flux at its output decreases rapidly with the distance. Consequently, the solar flux at the sample position can be controlled by modifying the distance between the output of the homogenization rod and the sample surface. To calibrate the flux at any position, we use a power meter mounted with a laser line filter at 632 nm.
A heating system with feedback is also incorporated into the sample holder in order to control the sample temperature during the experiment. We use a resistive wire sandwiched between two metallic plates that is powered through a PID regulator. The homogeneity of the temperature over the sample surface is checked by IR camera measurements (see Section A.3 of SI for a complete description of the sample holder and heating systems).

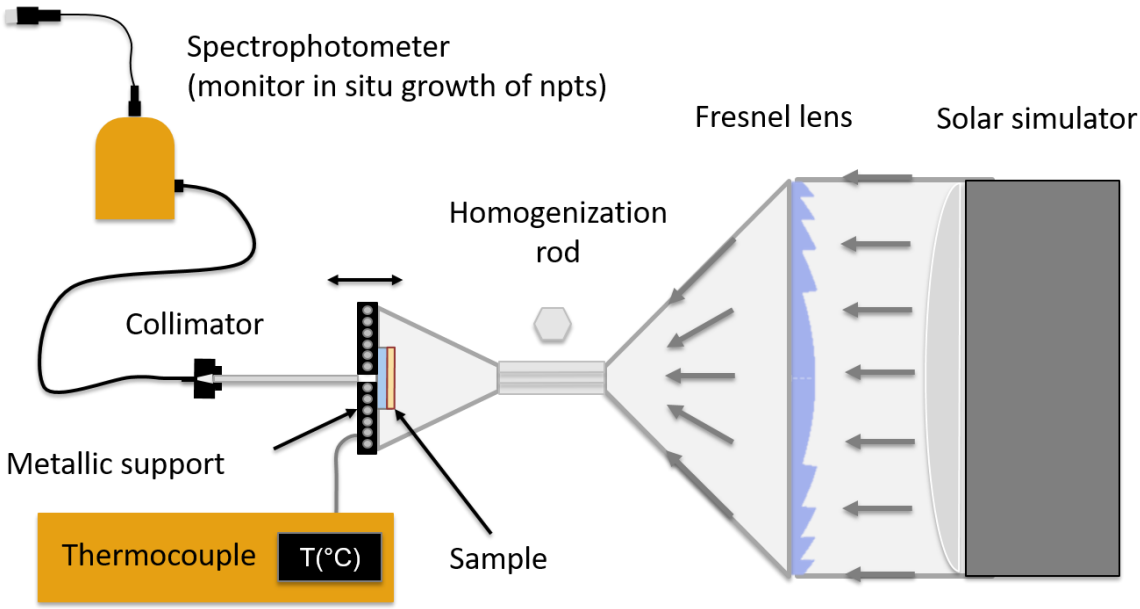

Figure 2:Experimental setup (detailed description is given in the main text)

Finally, an aperture (1.5 mm hole) at the center of the sample's holder allows for *in operando* measurements of absorption spectra of the composites during the synthesis under irradiation. This enables us to follow the nanoparticles growth in real time through the evolution of their plasmon resonance.

At the end of the elaboration procedure, the morphology, size distributions of the NPs were investigated by transmission electronic microscopy (TEM) in a JEOL JEM 1400. The TEM images were obtained from liquid samples, by dissolving the films locally after fabrication and depositing an aliquot on a carbon coated TEM grid. The nanoparticle size distributions have been measured over more than 300 nanoparticles of each sample.

The optical properties of the particles, and more especially the spatial electromagnetic field distribution around the nanoparticles were simulated by the MNPBEM software[47,48], using Johnson and Christy experimental values for the permittivity of gold and n=1.49 for the index PMMA.

Results and discussion

The series of PMMA films doped with chloroauric acid ($HAuCl_4$. $3H_2O$) have been prepared by using the same stock solution.

A first experiment was realized to evidence the effect of the CSI on the synthesis. For this, we irradiated one of the films at 50 suns (i.e. a concentration factor of 50) for 10 minutes, which naturally induces an increase of temperature. The absorption spectra and the temperature profile of the sample were measured *in situ* during the fabrication process, see Fig.3.(a) and (b) respectively. Due to the specific configuration of our experimental setup, which uses the same filtered solar beam for the irradiation of the samples and as a source for the absorption measurements, only the visible part of the spectra is exploitable. The spectra present an increasing peak in the 520-550 nm range, corresponding to the plasmon resonance of gold nanoparticles in polymer matrices with refractive index of 1.5[49]. We see that after 10 minutes, the temperature is stabilized around 130 °C, and the absorption spectra no longer change, which indicates that the system has reached stability.

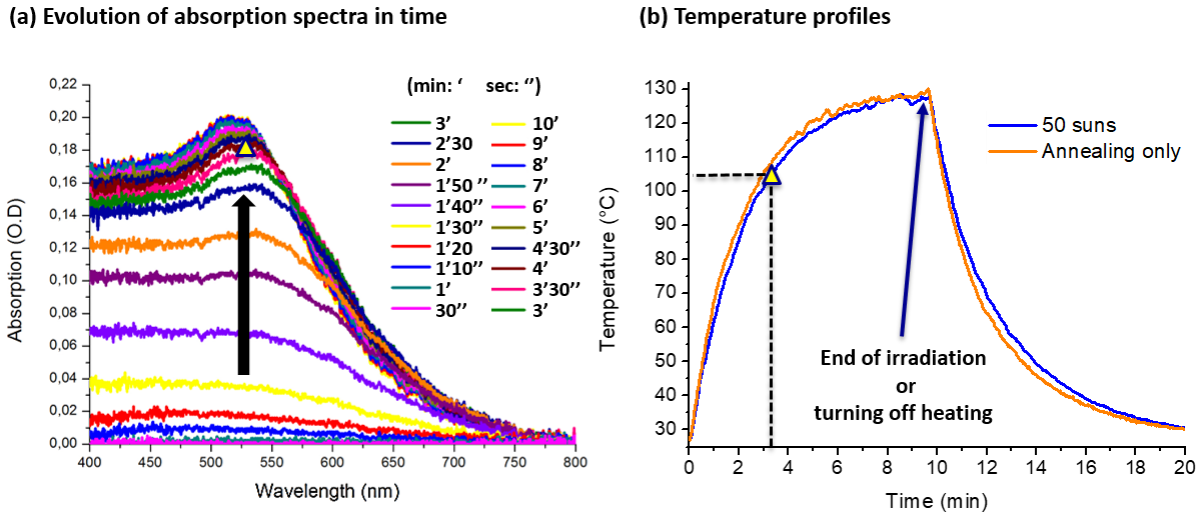

Figure 3: (a) In situ absorption spectra measured during the irradiation under 50 suns and (b) Temperature profiles during the synthesis for the sample irradiated at 50 suns (in blue) and the sample that has been annealed only (in orange). The synthesis duration is 10 min.

To discriminate the effect of irradiation from the annealing, a second identical sample was heated without using any irradiation, employing the same temperature profile as the one recorded during the experiment under irradiation, (orange trace in Fig.3.(b)). The optical spectra of the films after spin coating and after the reaction with or without irradiation are shown in Fig.4. After spin-coating, we observe an absorption peak centered at 320 nm attributed to $HAuCl_4$. For the irradiated sample, we see that the characteristic peak of the plasmon resonance of gold as appears around 520 nm, indicating the formation of gold nanoparticles. Moreover, the peak at 320 nm has disappeared, replaced by a large absorption band due to the inter-band transitions in metallic gold, which indicates that the gold precursor has been completely reduced. By contrast, the sample prepared by annealing shows no signature of Au nanoparticles. Moreover, the peak at 320 nm has decreased in intensity but

has not completely disappeared. This can be interpreted as a partial reduction of the gold precursor that did not lead to the formation of gold nanoparticles. Annealing in these conditions (130 °C for 10 min) is thus not sufficient to initiate nanoparticle growth in the PMMA. As expected, this first results indicates that the irradiation plays a major role in the photo-reduction of the metal salt.

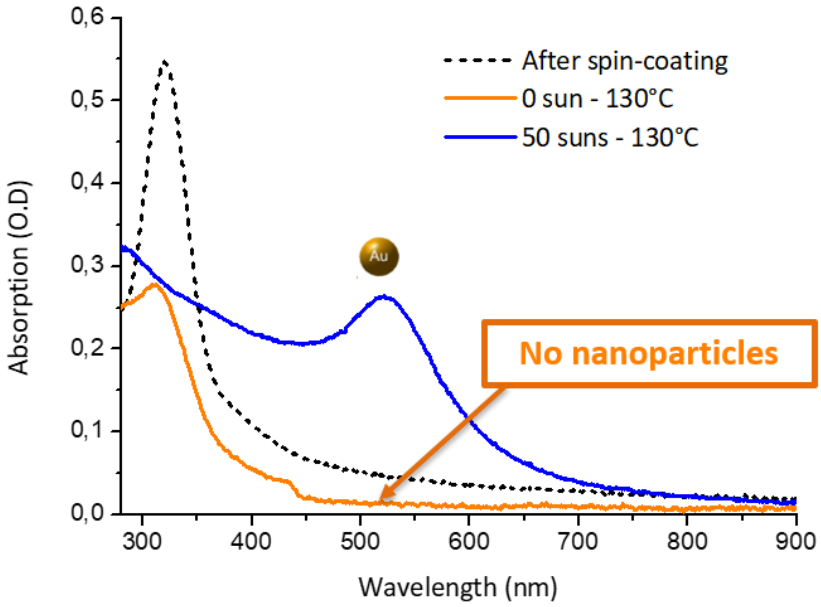

Figure 4: Absorption spectra of the Au/PMMA thin film after spin coating (black dotted line), and after irradiation at 50 suns and annealing at 130°C (blue line) or annealed at 130°C only (orange line)

We then investigated the effect of the irradiation flux by varying the concentration factor of light. For that, doped films were irradiated at various irradiation fluxes, respectively 1, 5, 15 and 30 suns. To focus on the effect of irradiation, we used the heating set-up to keep an identical temperature profiles for all experiments, so that the effect of annealing was similar in all cases. The reference profile was the temperature profile obtained by irradiating our sample at 50 suns without additional heating. The evolution of the temperature and the absorption spectra of the samples were measured during the experiment, see in Fig.5.

In order to compare the nanoparticle morphology in the different samples, we intentionally stopped the irradiation once the resonance peak was stable for several minutes. For solar flux higher than 5 suns, the spectra stopped evolving after 10 minutes. For 1 sun however, a longer time up to 20 minutes was necessary. The peaks might still evolve for much longer irradiation times (several hours maintaining the temperature of 130 °C) but we intentionally stopped the irradiation once the resonance peak was stable for several minutes in order to compare the nanoparticle morphology in the different samples. The optical spectra of such prepared samples are stable for months when exposed to ambient conditions of light and temperature. This seems to indicate in particular that at the end of the irradiation, the whole precursor amount has been reduced and converted to gold nanoparticles.

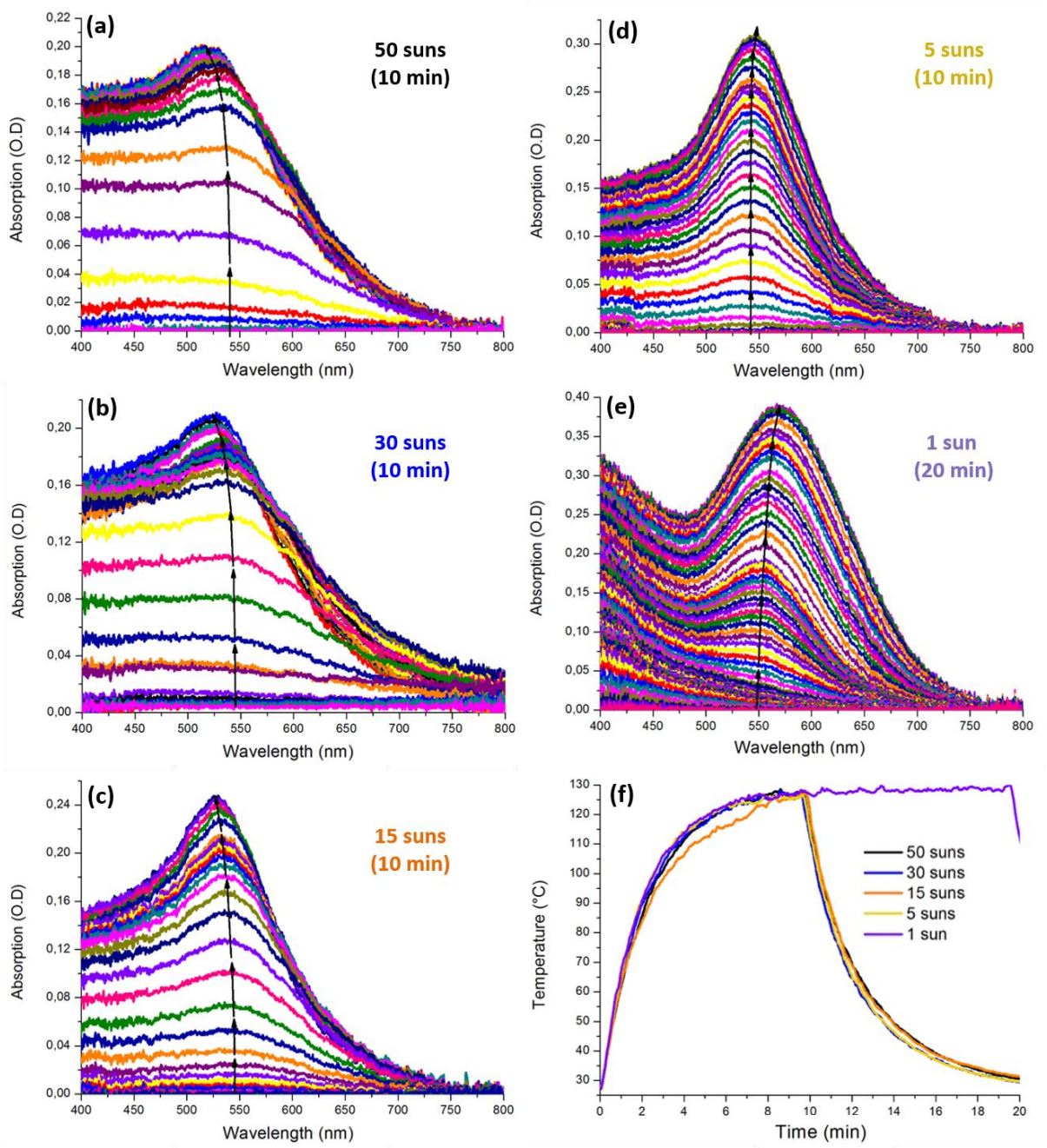

Figure 5: (a) to (e) Absorption spectra measured in situ during the synthesis at different solar fluxes (50, 30, 15, 5 and 1 sun) and (f) the corresponding temperature elevation profiles (f).

The TEM images along with the corresponding nanoparticle size distributions of the different nanocomposites are given in Fig. 6. These images show that it is possible to control the nanoparticle size distribution by changing the solar flux used for synthesis. Indeed, the average size of the nanoparticles is minimal at 50 suns (mean radius 3 nm) and progressively increases as the flux is decreased to reach a mean radius of 15 nm at 1 sun. Moreover, we observe that the nanoparticle shape is roughly spherical from 50 to 15 suns but then some facetted shapes start to appear at 5 suns. Finally, the sample at 1 sun presents a bimodal size distribution composed on one hand of rather large well facetted nanoparticles (nanocubes truncated octahedrons and triangular nanoprisms) and on the other of very small spherical nanoparticles with radius around 1.5 nm.

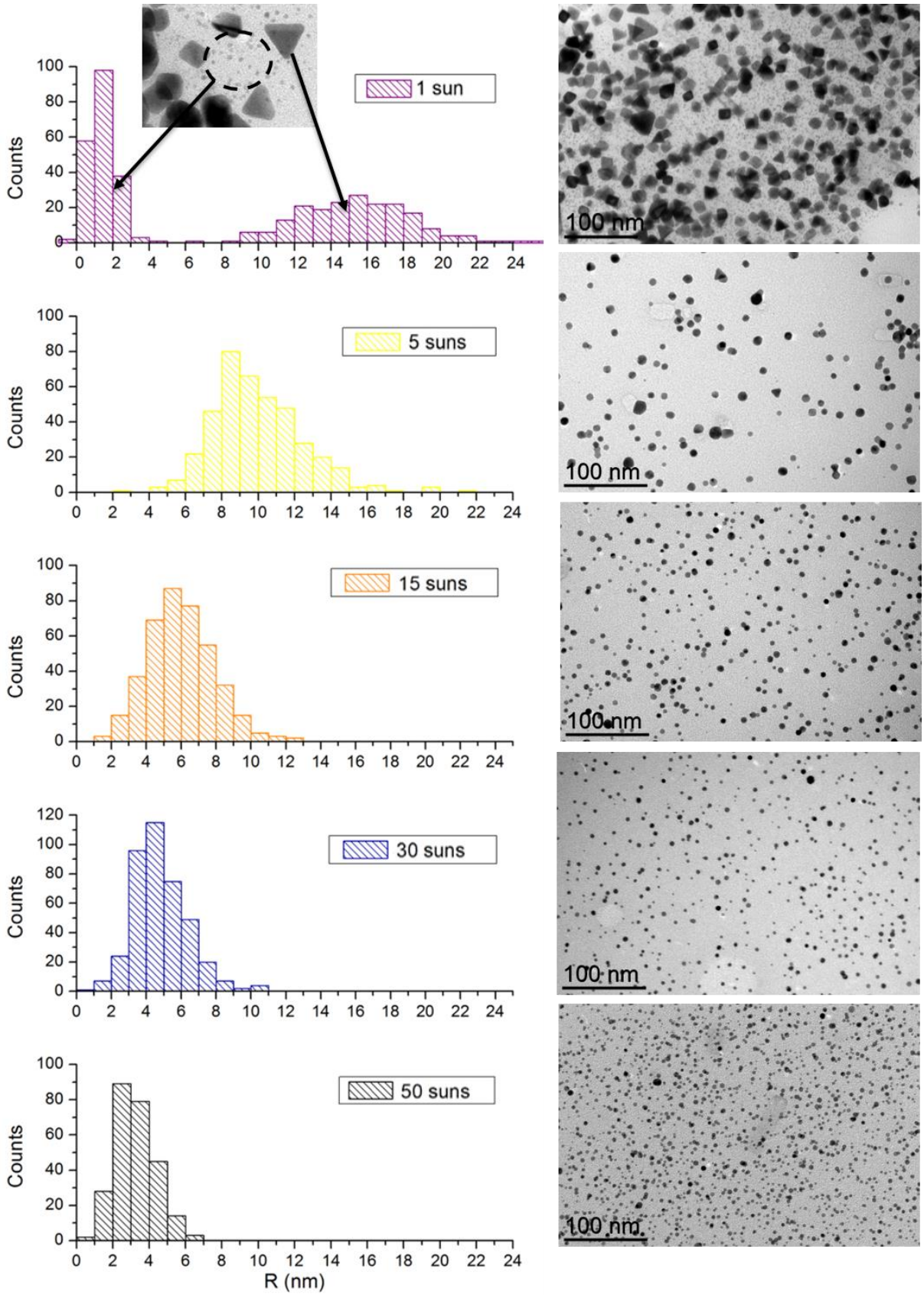

Figure 6: TEM images of the different samples irradiated from 1 to 50 suns (from top to bottom) and the corresponding nanoparticles radius distributions.

This size and shape evolution is accompanied by an evolution of the optical properties of the nanocomposites, and more precisely by a change in the position and amplitude of the plasmon resonance, see Fig. 7. The control of the solar flux thus makes it possible to control the position of the plasmonic peak from 519 nm at 50 suns to 566 nm at 1 sun.

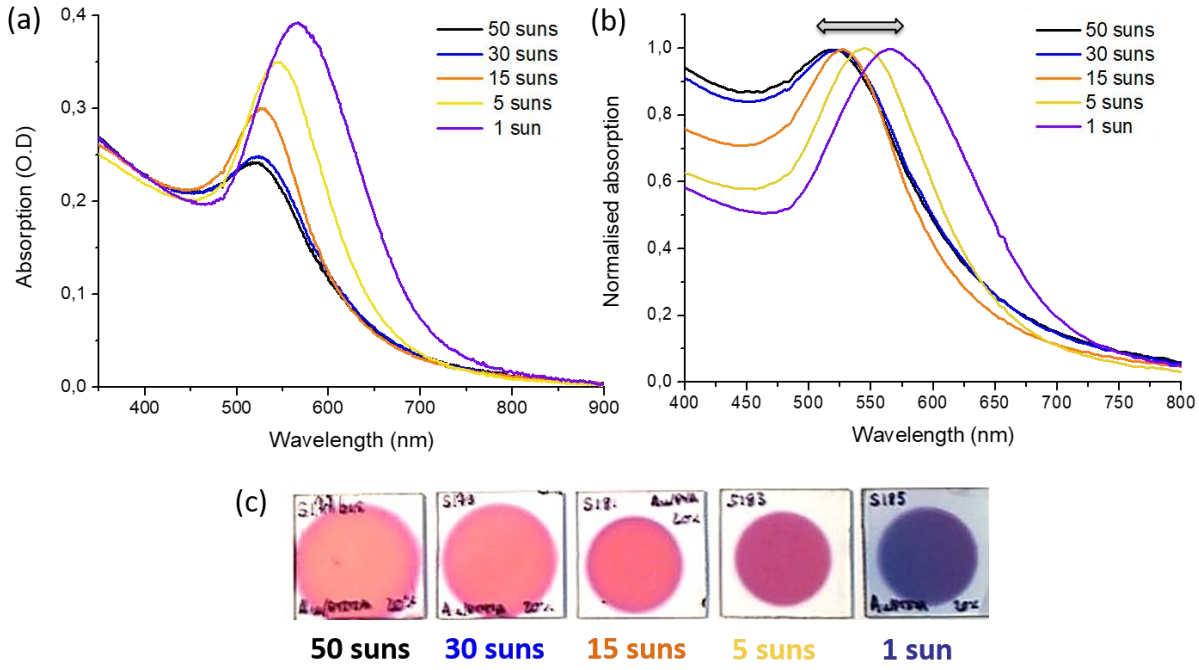

Figure 7: (a) Final absorption spectra of the different Au/PMMA nanocomposites prepared from 50 to 1 sun, (b) same spectra normalized to the maximum of the plasmon peak) and (c) photos of the corresponding sample

In order to better understand the formation of the nanoparticles with SCI, we analyzed the dynamical evolution of the absorption spectra during the synthesis. In Fig. 8, we plot the maximum of the plasmon peak as a function of time for the five samples. For the sake of comparison, the amplitudes were normalized with respect to the final amplitude. It is known that, for gold particles, the plasmon resonance appears only when the particle size reaches approximately 2 nm, and for moderate sizes (less than 20-30 nm), the plasmon peak intensity increases proportionally to the volume of the particle. An increase of the plasmon peak intensity may thus reflect either an increase of the particle number, or the growth of already-formed particles. As a consequence, the time evolution of the plasmon peak can help understanding the growth mechanisms of the particles. On the other hand, it does not inform on the photoreduction dynamics and the formation of objects smaller than 2 nm.

We clearly observe an acceleration of the nanoparticle growth kinetics when the irradiation flux increases. At high fluxes (more than 30 suns), the plasmon peak appears after about 1 min of irradiation, which means that the photoreduction and nucleation steps happen very rapidly. The amplitude of the plasmon peak then increases rapidly, indicating a fast growth of the nanoparticles, until a plateau is reached indicating that the metallic precursor has been consumed. In this case, small roughly spherical particles are obtained. These results can be interpreted in the frame of the La Mer mechanism, which is a very common growth mechanism in the chemical synthesis of inorganic nanoparticles[50] and especially nanospheres. A fast reduction provokes a fast supersaturation of the medium in active monomers leading

to a burst nucleation of a high number of seeds. This step consumes the majority of the Au reservoir in the nucleation step, which gives rise to seeds (enclosed by a mix of {111} and {100} facets, which is the thermodynamically favorable configuration[51]), that upon growing, give rise to nanoparticles of almost spherical shape. It is noticeable that most of the particle formation occurs before 3 min, i.e. before the glass transition temperature of the polymer is reached. This indicates that, once the precursor is reduced, the mobility of the gold atoms at low temperature is sufficient to lead to the formation of the nanoparticles.

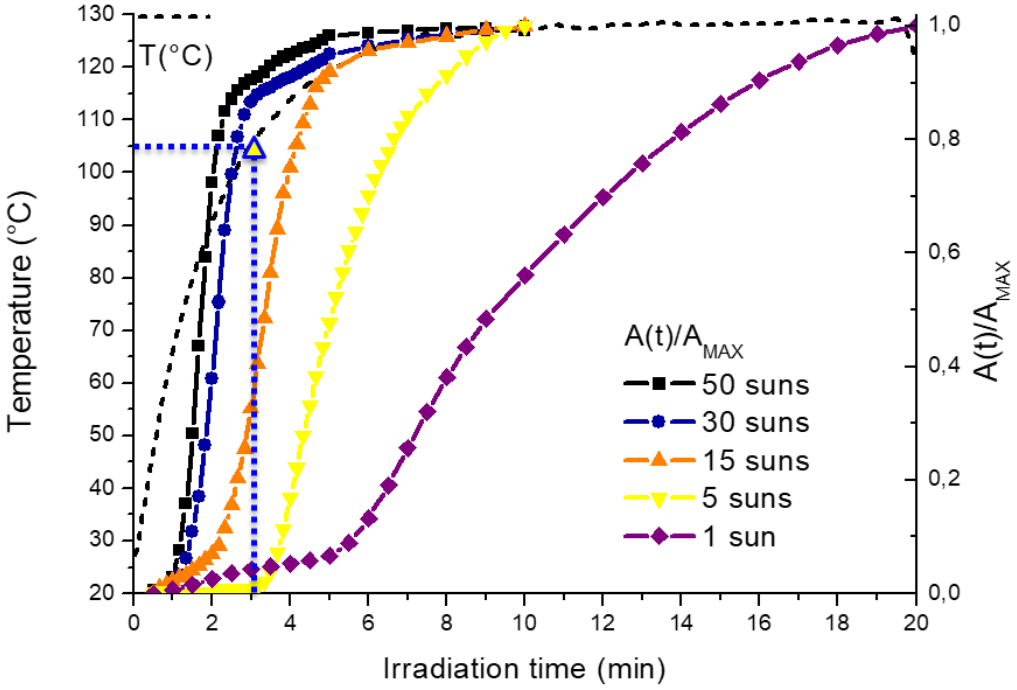

Figure 8: Typical temperature profile measured during the synthesis (left axis) along with the evolution of the normalized amplitude of the plasmon resonance peak during the irradiation (right axis) that describes the nanoparticle growth kinetics. The yellow triangle indicates the time at which the transition temperature of PMMA (105 °C) is reached.

At lower fluxes (1 and 5 suns), the kinetics are slower and less segmented. The increase of the absorption is more progressive and we assume that the photoreduction, nucleation and growth are slower. Moreover, especially at 1 sun we no longer form only spherical nanoparticles but the synthesis also leads to faceted shapes among which triangular prisms. Anisotropic growth is usually induced by using facet-selective ligands in order to block the access of theses facets and orientate the nanoparticle growth in preferential directions[52,53] However, the PMMA does not present a functional group susceptible to bind strongly to the nanoparticles surface[54] and it has been shown that, contrary to other halogen species, chlorine is not efficient for initiating anisotropic growth[55]. Consequently, the usual pathway for anisotropic growth are not easy to confirm in our system and other schemes should be considered.

Under low fluxes, the slow reduction kinetics lead to a less extended nucleation (fewer nuclei) on which, subsequent slow and extended growth favors the elimination of multiply twinned seeds, which are stable only at small sizes[42.] Thus, it is likely that the seeds that survive and further grow are either single crystalline giving rise to octahedra, tetrahedra, nanocubes, cuboctahedra or single twinned seeds which finally form triangular platelets. Indeed, it has been shown that slow reduction favors the formation of plate-like nanoparticles in fcc metals[56], which can explain the presence of nanoprisms growing from seeds comprising (111)

twin planes. Recently, the formation of Au nanoplates from $HAuCl_4$ under electron beam irradiation and in the absence of added stabilizers has been attributed to the slow reduction[57]. However, an open question is to which degree the plasmonic properties of the growing nanostructures assist anisotropic growth. Indeed, as it has been demonstrated by EELS spectroscopy, submitting plasmonic nanoparticles to an electron beam enables to excite the full set of plasmon resonance modes[58]. Similarly, one of the specificities of our approach is that the nanoparticles are irradiated with broadband irradiation during their growth and, therefore, their plasmon resonances are excited. Consequently, the electromagnetic field intensity is enhanced and its spatial distribution is modified at the vicinity of the nanoparticles, which can influence the growth process. This field, known as plasmon driven synthesis, has been extensively studied for the synthesis of silver nanoparticles in solution and only a few times for gold nanoparticles in solution[59,60]. As far as we know, this phenomenon has never been observed in the case of in situ synthesis in thin polymer films.

Baffou et al gave a detailed description of the different plasmon mediated mechanisms that could occur in such situations[61]. Among these mechanisms, two might explain an anisotropic growth of the nanoparticles. First, the local field enhancement, might directly influence the photoreduction and growth rates along specific directions. Moreover, exciting the plasmonic resonance results in the production of hot electrons, which could increase the reduction rate of the gold precursor locally. This local photoreduction would induce an inhomogeneity in the gold ions distribution in the bulk. As it has been previously observed in similar systems[37], gold precursors can then migrate toward depleted areas where the electromagnetic field intensity is maximal. This migration allows for a continuous renewal of the precursor population, feeding the anisotropic growth mechanisms. A schematic description of these mechanisms is proposed in Fig.9.

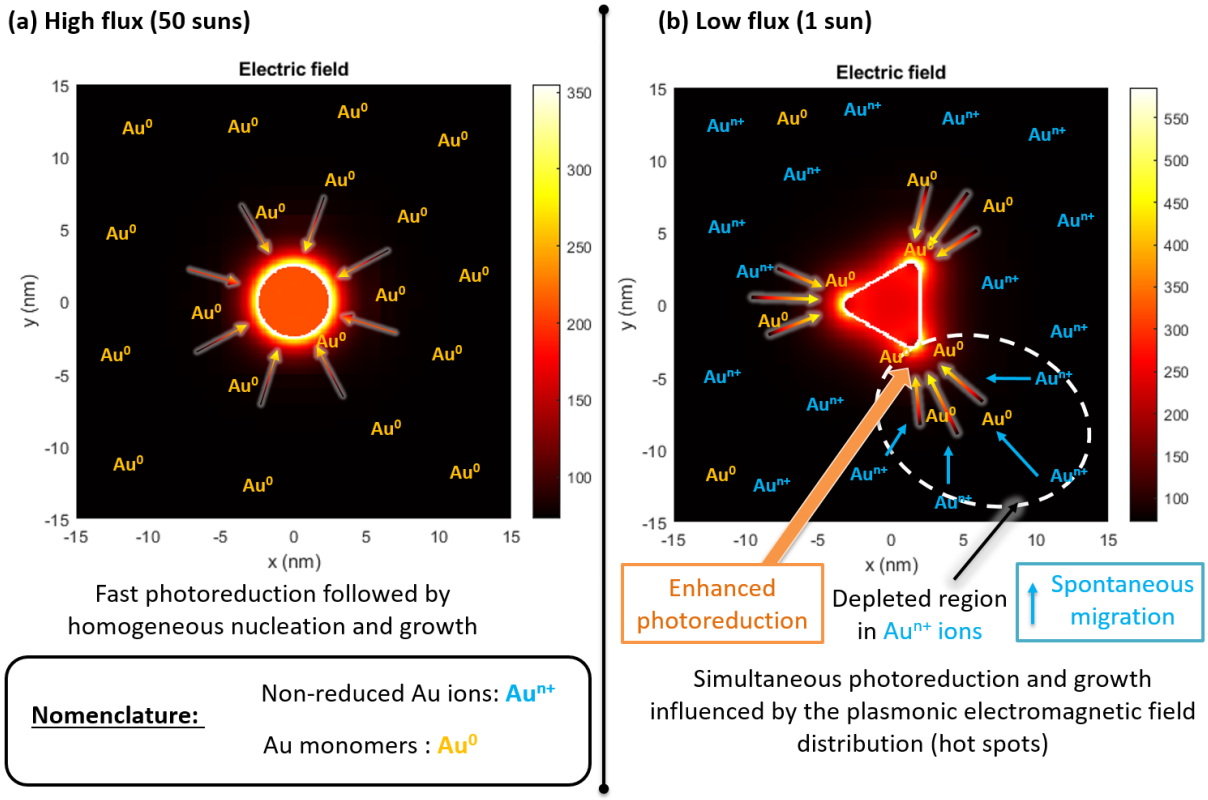

Figure 9: Scattered field map for (a) a nanospheres and (b) a nanoprism under non-polarized light along with schematic Illustrations of possible growth mechanisms: Homogenous nucleation and growth at high flux in (a) and anisotropic growth induced by plasmonic hot spots in (b).

In Fig. 9, the electromagnetic field distribution around the nanoparticle has been calculated by averaging the field maps obtained for different polarization angles such that it is representative of the non-polarized light that it is used in our setup. The simulation results show that in such conditions, the field enhancement is anisotropic around a sphere whereas it is maximal at all tips ends for a nanoprism (a similar result would be obtained for a nanocube). We assume that when the irradiation flux is low, the two effects, that are, slow reduction kinetics and plasmon assisted anisotropic growth, may account for the observed morphology. Indeed, while slow kinetics allow the initial formation of twin (111) planes on the nanoparticle seeds, further growth could be accelerated from plasmon active nanocrystals with anisotropic field distribution contributing to the anisotropic growth. This effect is not observed at high flux because the photoreduction happens too fast, followed by a homogenous nucleation and insufficient growth, ultimately leading to the formation of small spherical nanoparticles favored by thermodynamics.

Finally, in the framework of the development of green synthesis approaches, we have tried to apply our method to a biopolymer, namely potato STARCH, soluble in water. The procedure used was the same as with PMMA and we have shown the possibility to induce the formation under 50 suns (130 °C) of gold nanoparticles showing a sharp plasmon resonance peak around 540 nm. As a comparison, the sample prepared under the same annealing temperature but without CSI shows only a partial photoreduction (peak at 320 nm) and the plasmon peak is very weak and broadened, see Fig.10.

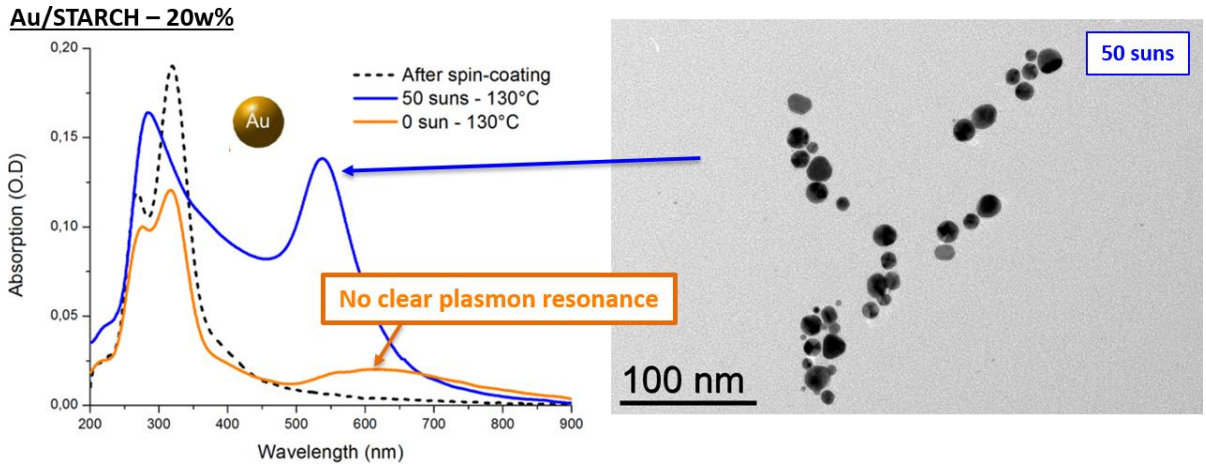

Figure 10: (left) Absorption spectra of the Au/STARCH nanocomposites after spin-coating, after 50 suns irradiations and after being annealed at 130°C without irradiation. (right) TEM image of the nanoparticles formed under 50 suns.

This result confirms the possibility to perform the green synthesis of Au/STARCH composite. It should be noted however that even if this synthesis, realized under 50 suns, leads to the formation of rather small nanoparticles (mean diameter ~ 10 nm, see Section B of SI) they are larger than what was observed in PMMA (mean diameter ~ 6 nm, see Fig.6). This behavior might be explained by the fact that the glass transition temperature of STRACH is significantly lower than PMMA (around 70 °C). Indeed, heating above the glass transition temperature facilitates the mobility of the gold monomers and may even induce coalescence of smaller nanoparticles during growth. More generally, the glass transition temperature certainly plays a role in the determination of nanoparticle size, and the growth kinetics might be controlled by heating the sample either just above or significantly above this threshold. Regarding the

nanoparticles shape, we assume that the glass transition temperature is not critical. As mentioned above, even if the monomers mobility might play a role in the growth mechanisms we believe that the nature of the polymer and more especially the type of functional groups it contains is the principal determining factor regarding the shape selectivity. In this case, it is the ability for the polymer to bounds selectively to specific Au facets that would induce anisotropy.
This last result demonstrates the versatility of the fabrication method but underlines the strong coupling between the polymer used and the growth mechanisms of the nanoparticles, which should be explored in more details.

Conclusions

In this study we have shown that concentrated solar irradiation can be used to perform an efficient one-step *in situ* synthesis of gold nanoparticles in PMMA and the bio-polymer potato starch. This demonstrates the versatility of this approach and shows its compatibility with green synthesis requirements. Furthermore, by controlling the solar flux and the sample temperature, we have been able to control the size distribution of the nanoparticles in the Au/PMMA nanocomposites and therefore their optical properties. By monitoring the evolution of the absorption spectra in time during the synthesis procedure, we could extract relevant information regarding the formation mechanisms of the nanoparticles and identify two different regimes at high and low flux. In particular, the results obtained at low fluxes (1 and 5 suns) suggest that slow reaction kinetics probably associated to a plasmon driven mechanism lead to the formation of facetted nanoparticles of different shapes such prisms. This last feature is of particular interest and should be investigated in more detail. In particular, a systematic study of the effect of both the light polarization and spectral distribution is planned to understand the role of plasmonic field enhancement on the growth mechanisms.
To summarize, we have shown that *in situ* synthesis of nanoparticles in polymer films under CSI seems to be a simple and promising technique to fabricate nanocomposites thin films in one step and with controlled morphologies. Regarding the potential applications, the setup we used for irradiation at 50 suns, that is a low concentration factor in the field of concentrated solar technology[49,50], can readily be up-scaled for the continuous production of nanocomposites on large areas.

References

(1) Li, S.; Meng Lin, M.; Toprak, M. S.; Kim, D. K.; Muhammed, M. Nanocomposites of Polymer and Inorganic Nanoparticles for Optical and Magnetic Applications. *Nano Rev.* **2010**, *1* (1), 5214. https://doi.org/10.3402/nano.v1i0.5214.

(2) Mei, L.; Lu, Z.; Zhang, X.; Li, C.; Jia, Y. Polymer-Ag Nanocomposites with Enhanced Antimicrobial Activity against Bacterial Infection. *ACS Appl. Mater. Interfaces* **2014**, *6* (18), 15813–15821. https://doi.org/10.1021/am502886m.

(3) Lee, S. Y.; Jeon, H. C.; Yang, S.-M. Unconventional Methods for Fabricating Nanostructures toward High-Fidelity Sensors. *J. Mater. Chem.* **2012**, *22* (13), 5900. https://doi.org/10.1039/c2jm16568f.

(4) Xiao, T.; Huang, J.; Wang, D.; Meng, T.; Yang, X. Au and Au-Based Nanomaterials: Synthesis and Recent Progress in Electrochemical Sensor Applications. *Talanta*. Elsevier

January 1, 2020, p 120210. https://doi.org/10.1016/j.talanta.2019.120210.
(5) Zhang, Q.; Chen, C.; Wan, G.; Lei, M.; Chi, M.; Wang, S.; Min, D. Solar Light Induced Synthesis of Silver Nanoparticles by Using Lignin as a Reductant, and Their Application to Ultrasensitive Spectrophotometric Determination of Mercury(II). *Microchim. Acta* **2019**, *186* (11), 727. https://doi.org/10.1007/s00604-019-3832-8.
(6) Zhang, Q.; Xie, G.; Xu, M.; Su, Y.; Tai, H.; Du, H.; Jiang, Y. Visible Light-Assisted Room Temperature Gas Sensing with ZnO-Ag Heterostructure Nanoparticles. *Sensors Actuators B Chem.* **2018**, *259*, 269–281. https://doi.org/10.1016/J.SNB.2017.12.052.
(7) Pastoriza-Santos, I.; Kinnear, C.; Pérez-Juste, J.; Mulvaney, P.; Liz-Marzán, L. M. Plasmonic Polymer Nanocomposites. *Nat. Rev. Mater.* **2018**, *3* (10), 375–391. https://doi.org/10.1038/s41578-018-0050-7.
(8) Hedayati, M. K.; Faupel, F.; Elbahri, M. Review of Plasmonic Nanocomposite Metamaterial Absorber. *Materials (Basel).* **2014**, *7* (2), 1221–1248. https://doi.org/10.3390/ma7021221.
(9) Malafronte, A.; Capretti, A.; Pepe, G. P.; Forestiere, C.; Miano, G.; Auriemma, F.; De Rosa, C.; Di Girolamo, R. Simple Theoretical Considerations for Block-Copolymer-Based Plasmonic Metamaterials. In *Macromolecular Symposia*; 2016; Vol. 359, pp 72–78. https://doi.org/10.1002/masy.201400178.
(10) Cheng, H.; Fuku, K.; Kuwahara, Y.; Mori, K.; Yamashita, H. Harnessing Single-Active Plasmonic Nanostructures for Enhanced Photocatalysis under Visible Light. *J. Mater. Chem. A* **2015**, *3* (10), 5244–5258. https://doi.org/10.1039/C4TA06484D.
(11) Kim, Y.; Smith, J. G.; Jain, P. K. Harvesting Multiple Electron–Hole Pairs Generated through Plasmonic Excitation of Au Nanoparticles. *Nat. Chem.* **2018**, *10* (7), 763–769. https://doi.org/10.1038/s41557-018-0054-3.
(12) Ma, X.-C.; Dai, Y.; Yu, L.; Huang, B.-B. Energy Transfer in Plasmonic Photocatalytic Composites. *Light Sci. Appl.* **2016**, *5* (April 2015). https://doi.org/10.1038/lsa.2016.17.
(13) Xu, M.; Chen, Y.; Hu, W. Y.; Liu, Y. T.; Zhang, Q. P.; Yuan, H.; Wang, X. Y.; Zhang, J. X.; Luo, K. Y.; Li, J.; et al. Designed Synthesis of Microstructure and Defect-Controlled Cu-Doped ZnO–Ag Nanoparticles: Exploring High-Efficiency Sunlight-Driven Photocatalysts. *J. Phys. D. Appl. Phys.* **2020**, *53* (2), 025106. https://doi.org/10.1088/1361-6463/ab4bfd.
(14) Atwater, H. A.; Polman, A. Plasmonics for Improved Photovoltaic Devices. *Nat. Mater.* **2010**, *9* (3), 205–213. https://doi.org/10.1038/nmat2629.
(15) Chen, X.; Zuo, L.; Fu, W.; Yan, Q.; Fan, C.; Chen, H. Insight into the Efficiency Enhancement of Polymer Solar Cells by Incorporating Gold Nanoparticles. *Sol. Energy Mater. Sol. Cells* **2013**, *111*, 1–8. https://doi.org/10.1016/j.solmat.2012.12.016.
(16) Stratakis, E.; Kymakis, E. Nanoparticle-Based Plasmonic Organic Photovoltaic Devices. *Materials Today*. 2013, pp 133–146. https://doi.org/10.1016/j.mattod.2013.04.006.
(17) Notarianni, M.; Vernon, K.; Chou, A.; Aljada, M.; Liu, J.; Motta, N. Plasmonic Effect of Gold Nanoparticles in Organic Solar Cells. *Sol. Energy* **2014**, *106*, 23–37. https://doi.org/10.1016/j.solener.2013.09.026.
(18) Kalfagiannis, N.; Karagiannidis, P. G.; Pitsalidis, C.; Panagiotopoulos, N. T.; Gravalidis, C.; Kassavetis, S.; Patsalas, P.; Logothetidis, S. Plasmonic Silver Nanoparticles for Improved Organic Solar Cells. *Sol. Energy Mater. Sol. Cells* **2012**, *104*, 165–174. https://doi.org/10.1016/j.solmat.2012.05.018.
(19) Wang, J. Y.; Hsu, F. C.; Huang, J. Y.; Wang, L.; Chen, Y. F. Bifunctional Polymer Nanocomposites as Hole-Transport Layers for Efficient Light Harvesting: Application to

Perovskite Solar Cells. *ACS Appl. Mater. Interfaces* **2015**, *7* (50), 27676–27684. https://doi.org/10.1021/acsami.5b08157.

(20) El-Bashir, S. M.; Barakat, F. M.; AlSalhi, M. S. Double Layered Plasmonic Thin-Film Luminescent Solar Concentrators Based on Polycarbonate Supports. *Renew. Energy* **2014**, *63*, 642–649. https://doi.org/10.1016/j.renene.2013.10.014.

(21) Mateen, F.; Oh, H.; Jung, W.; Binns, M.; Hong, S. K. Metal Nanoparticles Based Stack Structured Plasmonic Luminescent Solar Concentrator. *Sol. Energy* **2017**, *155*, 934–941. https://doi.org/10.1016/j.solener.2017.07.037.

(22) Hsu, S.-W.; Rodarte, A. L.; Som, M.; Arya, G.; Tao, A. R. Colloidal Plasmonic Nanocomposites: From Fabrication to Optical Function. *Chem. Rev.* **2018**, acs.chemrev.7b00364. https://doi.org/10.1021/acs.chemrev.7b00364.

(23) Daruich De Souza, C.; Ribeiro Nogueira, B.; Rostelato, M. E. C. M. Review of the Methodologies Used in the Synthesis Gold Nanoparticles by Chemical Reduction. *J. Alloys Compd.* **2019**, *798*, 714–740. https://doi.org/10.1016/J.JALLCOM.2019.05.153.

(24) Liu, K.; He, Z.; Curtin, J. F.; Byrne, H. J.; Tian, F. A Novel, Rapid, Seedless, in Situ Synthesis Method of Shape and Size Controllable Gold Nanoparticles Using Phosphates. *Sci. Rep.* **2019**, *9* (1), 7421. https://doi.org/10.1038/s41598-019-43921-0.

(25) Van Patten, P. G. Metal-Polymer Nanocomposites. *J. Am. Chem. Soc.* **2005**, *127* (15), 5728. https://doi.org/10.1021/ja041000s.

(26) SETHI, A.; Rafiee, M.; Chandra, S.; Ahmed, H.; McCormack, S. A Unified Methodology for Fabrication and Quantification of Gold Nanorods, Gold Core Silver Shell Nanocuboids and Their Polymer Nanocomposites. *Langmuir* **2019**, acs.langmuir.9b01481. https://doi.org/10.1021/acs.langmuir.9b01481.

(27) Kraynov, A.; Müller, T. Concepts for the Stabilization of Metal Nanoparticles in Ionic Liquids. *Appl. Ion. Liq. Sci. Technol.* **2011**, 1–27. https://doi.org/10.5772/1769.

(28) Ghosh, S. K.; Pal, T. Interparticle Coupling Effect on the Surface Plasmon Resonance of Gold Nanoparticles: From Theory to Applications. *Chem. Rev.* **2007**, *107* (11), 4797–4862. https://doi.org/10.1021/cr0680282.

(29) Hasell, T.; Lagonigro, L.; Peacock, A. C.; Yoda, S.; Brown, P. D.; Sazio, P. J. A.; Howdle, S. M. Silver Nanoparticle Impregnated Polycarbonate Substrates for Surface Enhanced Raman Spectroscopy. *Adv. Funct. Mater.* **2008**, *18* (8), 1265–1271. https://doi.org/10.1002/adfm.200701429.

(30) Sohn, B.-H.; Seo, B.-W.; Yoo, S.-I. Changes of the Lamellar Period by Nanoparticles in the Nanoreactor Scheme of Thin Films of Symmetric Diblock Copolymers. *J. Mater. Chem.* **2002**, *12* (6), 1730–1734. https://doi.org/10.1039/b201752k.

(31) Sandra Rifai; Craig A. Breen, †; Daniel J. Solis, † and; Swager*, T. M. Facile in Situ Silver Nanoparticle Formation in Insulating Porous Polymer Matrices. **2005**. https://doi.org/10.1021/CM0511419.

(32) Porel, S.; Singh, S.; Radhakrishnan, T. P. Polygonal Gold Nanoplates in a Polymer Matrix. *Chem. Commun. (Camb).* **2005**, No. 18, 2387–2389. https://doi.org/10.1039/b500536a.

(33) Porel, S.; Venkatram, N.; Rao, D. N.; Radhakrishnan, T. P. In Situ Synthesis of Metal Nanoparticles in Polymer Matrix and Their Optical Limiting Applications. *J. Nanosci. Nanotechnol.* **2007**, *7* (6), 1887–1892.

(34) Saikia, R.; Gogoi, P.; Barua, P. K.; Datta, P. SPECTROSCOPIC STUDIES ON Ag/PVA NANOCOMPOSITE THIN FILMS PREPARED BY THERMAL ANNEALING PROCESS. *Int. J. Nanosci.* **2011**, *10* (03), 427–432. https://doi.org/10.1142/S0219581X11008174.

(35) Alexandrov, A.; Smirnova, L.; Yakimovich, N.; Sapogova, N.; Soustov, L.; Kirsanov, A.;

Bityurin, N. UV-Initiated Growth of Gold Nanoparticles in PMMA Matrix. *Appl. Surf. Sci.* **2005**, *248* (1–4), 181–184. https://doi.org/10.1016/j.apsusc.2005.03.002.

(36) Abyaneh, M. K.; Paramanik, D.; Varma, S.; Gosavi, S. W.; Kulkarni, S. K. Formation of Gold Nanoparticles in Polymethylmethacrylate by UV Irradiation. *J. Phys. D. Appl. Phys.* **2007**, *40* (12), 3771–3779. https://doi.org/10.1088/0022-3727/40/12/032.

(37) Yilmaz, E.; Ertas, G.; Bengu, E.; Suzer, S. Photopatterning of PMMA Films with Gold Nanoparticles: Diffusion of Au Cl 4 - Ions. *J. Phys. Chem. C* **2010**, *114* (43), 18401–18406. https://doi.org/10.1021/jp106672f.

(38) Kassaee, M. Z.; Mohammadkhani, M.; Akhavan, a.; Mohammadi, R. In Situ Formation of Silver Nanoparticles in PMMA via Reduction of Silver Ions by Butylated Hydroxytoluene. *Struct. Chem.* **2011**, *22* (1), 11–15. https://doi.org/10.1007/s11224-010-9671-1.

(39) Balan, L.; Malval, J.; Lougnot, D. In Situ Photochemically Assisted Synthesis of Silver Nanoparticles in Polymer Matrixes. *Intech Open* **2009**, No. 4, 79–92.

(40) Balan, L.; Schneider, R.; Turck, C.; Lougnot, D.; Morlet-Savary, F. Photogenerating Silver Nanoparticles and Polymer Nanocomposites by Direct Activation in the near Infrared. *J. Nanomater.* **2012**, *2012*. https://doi.org/10.1155/2012/512579.

(41) Nadal, E.; Barros, N.; Glénat, H.; Laverdant, J.; Schmool, D. S.; Kachkachi, H. Plasmon-Enhanced Diffraction in Nanoparticle Gratings Fabricated by in Situ Photo-Reduction of Gold Chloride Doped Polymer Thin Films by Laser Interference Patterning. *J. Mater. Chem. C* **2017**, *5* (14), 3553–3560. https://doi.org/10.1039/C7TC00061H.

(42) Laplaze, D.; Bernier, P.; Flamant, G.; Lebrun, M.; Brunelle, A.; Della-Negra, S. Solar Energy: Application to the Production of Fullerenes. *J. Phys. B At. Mol. Opt. Phys.* **1996**, *29* (21), 4943–4954. https://doi.org/10.1088/0953-4075/29/21/008.

(43) Alvarez, L.; Guillard, T.; Sauvajol, J. L.; Flamant, G.; Laplaze, D. Solar Production of Single-Wall Carbon Nanotubes: Growth Mechanisms Studied by Electron Microscopy and Raman Spectroscopy. *Appl. Phys. A Mater. Sci. Process.* **2000**, *70* (2), 169–173. https://doi.org/10.1007/s003390050029.

(44) Brontvein, O.; Stroppa, D. G.; Popovitz-Biro, R.; Albu-Yaron, A.; Levy, M.; Feuerman, D.; Houben, L.; Tenne, R.; Gordon, J. M. New High-Temperature Pb-Catalyzed Synthesis of Inorganic Nanotubes. *J. Am. Chem. Soc.* **2012**, *134* (39), 16379–16386. https://doi.org/10.1021/ja307043w.

(45) Katz, E. A.; Visoly-fisher, I.; Feuermann, D.; Tenne, R.; Gordon, J. M. Concentrated Sunlight for Materials Synthesis and Diagnostics. *Adv. Mater.* **2018**, *1800444*, 1–10. https://doi.org/10.1002/adma.201800444.

(46) Albu-Yaron, A.; Levy, M.; Tenne, R.; Popovitz-Biro, R.; Weidenbach, M.; Bar-Sadan, M.; Houben, L.; Enyashin, A. N.; Seifert, G.; Feuermann, D.; et al. MoS2 Hybrid Nanostructures: From Octahedral to Quasi-Spherical Shells within Individual Nanoparticles. *Angew. Chemie - Int. Ed.* **2011**, *50* (8), 1810–1814. https://doi.org/10.1002/anie.201006719.

(47) Hohenester, U.; Trügler, A. MNPBEM - A Matlab Toolbox for the Simulation of Plasmonic Nanoparticles. *Comput. Phys. Commun.* **2012**, *183* (2), 370–381.

(48) Hohenester, U.; Trügler, A. MNPBEM - A Matlab Toolbox for the Simulation of Plasmonic Nanoparticles. **2011**.

(49) Enoch, S.; Bonod, N. *Plasmonics: From Basics to Advanced Topics*; Stefan Enoch (Institut Fresnel, CNRS), Nicolas Bonod (Institut Fresnel, C., Ed.; Springer, 2012; Vol. 167.

(50) Thanh, N. T. K.; Maclean, N.; Mahiddine, S. Mechanisms of Nucleation and Growth of

Nanoparticles in Solution. *Chem. Rev.* **2014**, *114* (15), 7610–7630. https://doi.org/10.1021/cr400544s.

(51) Xia, Y.; Xiong, Y.; Lim, B.; Skrabalak, S. E. Shape-Controlled Synthesis of Metal Nanocrystals : Simple Chemistry Meets Complex Physics? *Angew. Chemie Int. Ed.* **2009**, *48* (1), 60–103. https://doi.org/10.1002/anie.200802248.Shape-Controlled.

(52) Park, J. E.; Lee, Y.; Nam, J. M. Precisely Shaped, Uniformly Formed Gold Nanocubes with Ultrahigh Reproducibility in Single-Particle Scattering and Surface-Enhanced Raman Scattering. *Nano Lett.* **2018**, *18* (10), 6475–6482. https://doi.org/10.1021/acs.nanolett.8b02973.

(53) Langille, M. R.; Personick, M. L.; Zhang, J.; Mirkin, C. A. Defining Rules for the Shape Evolution of Gold Nanoparticles. *J. Am. Chem. Soc.* **2012**, *134* (35), 14542–14554. https://doi.org/10.1021/ja305245g.

(54) Sperling, R. A.; Parak, W. J. Surface Modification, Functionalization and Bioconjugation of Colloidal Inorganic Nanoparticles. *Philos. Trans. R. Soc. A Math. Phys. Eng. Sci.* **2010**, *368* (1915), 1333–1383. https://doi.org/10.1098/rsta.2009.0273.

(55) Duchene, J. S.; Niu, W.; Abendroth, J. M.; Sun, Q.; Zhao, W.; Huo, F.; Wei, W. D. Halide Anions as Shape-Directing Agents for Obtaining High-Quality Anisotropic Gold Nanostructures. *Chem. Mater.* **2013**, *25* (8), 1392–1399. https://doi.org/10.1021/cm3020397.

(56) Xiong, Y.; Chen, J.; Wiley, B.; Xia, Y.; Aloni, S.; Yin, Y. Understanding the Role of Oxidative Etching in the Polyol Synthesis of Pd Nanoparticles with Uniform Shape and Size. *J. Am. Chem. Soc.* **2005**, *127* (20), 7332–7333. https://doi.org/10.1021/ja0513741.

(57) Alloyeau, D.; Dachraoui, W.; Javed, Y.; Belkahla, H.; Wang, G.; Lecoq, H.; Ammar, S.; Ersen, O.; Wisnet, A.; Gazeau, F.; et al. Unravelling Kinetic and Thermodynamic Effects on the Growth of Gold Nanoplates by Liquid Transmission Electron Microscopy. *Nano Lett.* **2015**, *15* (4), 2574–2581. https://doi.org/10.1021/acs.nanolett.5b00140.

(58) Wu, Y.; Li, G.; Camden, J. P. Probing Nanoparticle Plasmons with Electron Energy Loss Spectroscopy. *Chem. Rev.* **2018**, *118* (6), 2994–3031. https://doi.org/10.1021/acs.chemrev.7b00354.

(59) Zhai, Y.; DuChene, J. S.; Wang, Y.-C.; Qiu, J.; Johnston-Peck, A. C.; You, B.; Guo, W.; DiCiaccio, B.; Qian, K.; Zhao, E. W.; et al. Polyvinylpyrrolidone-Induced Anisotropic Growth of Gold Nanoprisms in Plasmon-Driven Synthesis. *Nat. Mater.* **2016**, *15* (8), 889–895. https://doi.org/10.1038/nmat4683.

(60) Watanabe, M.; Araki, S.; Hayashi, K. Directed Growth of Metal Nanoparticles on Substrates by Polarized Light Irradiation. *2015 Ieee Sensors* **2015**, 1–4. https://doi.org/10.1109/ICSENS.2015.7370643.

(61) Baffou, G.; Quidant, R. Nanoplasmonics for Chemistry. *Chem. Soc. Rev.* **2014**, *43* (11), 3898–3907. https://doi.org/10.1039/c3cs60364d.